Astronomy & Astrophysics manuscript no. OC_carrera_CaT_v2
April 24, 2015

Radial velocities and metallicities from infrared Ca II triplet spectroscopy of open clusters

II. Berkeley 23, King 1, NGC 559, NGC 6603, and NGC 7245⋆

R. Carrera[1, 2], L. Casamiquela[3], N. Ospina[4], L. Balaguer-Núñez[3], C. Jordi[3], and L. Monteagudo[1, 2]

[1] Instituto de Astrofísica de Canarias, La Laguna, Tenerife, Spain
e-mail: rcarrera@iac.es
[2] Departamento de Astrofísica, Universidad de La Laguna, Tenerife, Spain
[3] Departament d'Astronomia i Meteorologia, Universitat de Barcelona, ICC/IEEC, Barcelona, Spain
[4] Institut de Ciències de l'Espai (CSIC-IEEC), Campus UAB, Bellaterra, Spain

Received September 15, 1996; accepted March 16, 1997

ABSTRACT

Context. Open clusters are key to studying the formation and evolution of the Galactic disc. However, there is a deficiency of radial velocity and chemical abundance determinations for open clusters in the literature.
Aims. We intend to increase the number of determinations of radial velocities and metallicities from spectroscopy for open clusters.
Methods. We acquired medium-resolution spectra ($R \sim 8000$) in the infrared region Ca II triplet lines (~8500 Å) for several stars in five open clusters with the long-slit IDS spectrograph on the 2.5 m Isaac Newton Telescope (Roque de los Muchachos Observatory, Spain). Radial velocities were obtained by cross-correlation fitting techniques. The relationships available in the literature between the strength of infrared Ca II lines and metallicity were also used to derive the metallicity for each cluster.
Results. We obtain $\langle V_r \rangle$ = 48.6 ± 3.4, −58.4 ± 6.8, 26.0 ± 4.3, and −65.3 ± 3.2 km s^{-1} for Berkeley 23, NGC 559, NGC 6603, and NGC 7245, respectively. We found [Fe/H]= −0.25 ± 0.14 and −0.15 ± 0.18 for NGC 559 and NGC 7245, respectively. Berkeley 23 has low metallicity, [Fe/H] = −0.42 ± 0.13, which is similar to other open clusters in the outskirts of the Galactic disc. In contrast, we derived high metallicity ([Fe/H] = +0.43 ± 0.15) for NGC 6603, which places this system amongst the most metal-rich known open clusters. To our knowledge, this is the first determination of radial velocities and metallicities from spectroscopy for these clusters, except NGC 6603, for which radial velocities had been previously determined. We have also analysed ten stars in the line of sight to King 1. Because of the large dispersion obtained in both radial velocity and metallicity, we cannot be sure that we have sampled true cluster members.

Key words. Stars: abundances – Galaxy: disc – Galaxy: open clusters and associations: individual: Berkeley 23; King 1; NGC 559; NGC 6603; NGC 7245

1. Introduction

Stellar clusters are crucial to the study of a variety of topics, including the star formation process, stellar nucleosynthesis and evolution, dynamical interaction among stars, and the assembly and evolution of galaxies. In particular, open clusters (OCs), which cover a wide range of ages and metallicities, have been widely used to constrain the formation and evolution of the Milky Way, and more specifically of the Galactic disc (e.g. Pancino et al. 2010; Frinchaboy et al. 2013). This is because some of their features, such as ages and distances, can be more accurately determined than for field stars.

Open clusters are therefore among the most important targets of ongoing and forthcoming Galactic surveys. The *Gaia* mission (Perryman et al. 2001; Mignard 2005; Lindegren 2005), for example, will provide accurate parallaxes and proper motions for all stars down to magnitude 20. Low- and medium-resolution spectroscopic surveys, such as the RAdial Velocity Experiment (RAVE; Conrad et al. 2014) and the Sloan Extension for Galactic Understanding and Exploration (SEGUE; Lee et al. 2008), provide radial velocities, together with some information about the chemical content of the stars. High-resolution spectroscopic surveys, such as the Apache Point Observatory Galactic Evolution Experiment (APOGEE; Frinchaboy et al. 2013), the Gaia-ESO Survey (GES; Donati et al. 2014) and GALactic Archaeology with HERMES (GALAH; Anguiano et al. 2014), supply accurate radial velocities and detailed chemical abundances. Additionally, some projects have been designed specifically to only investigate open clusters. For example, the Bologna Open Clusters Chemical Evolution project (BOCCE; Bragaglia & Tosi 2006) uses both comparison between observed colour-magnitude diagrams and stellar evolutionary models, and the analysis of high-resolution spectra to infer cluster properties such as age, distance, and chemical composition. Another survey devoted exclusively to OCs is Open cluster Chemical Abundances from Spanish Observatories (OCCASO; Carrera et al. 2014). Following a similar strategy to GES, this survey obtains accurate radial velocities and chemical abundances from high-resolution spectroscopy. Taken together, these surveys will pro-

⋆ Based on observations made with the 2.5 Isaac Newton Telescope operated on the island of La Palma by the Isaac Newton Group in the Spanish Observatorio del Roque de los Muchachos of the Instituto de Astrofísica de Canarias.

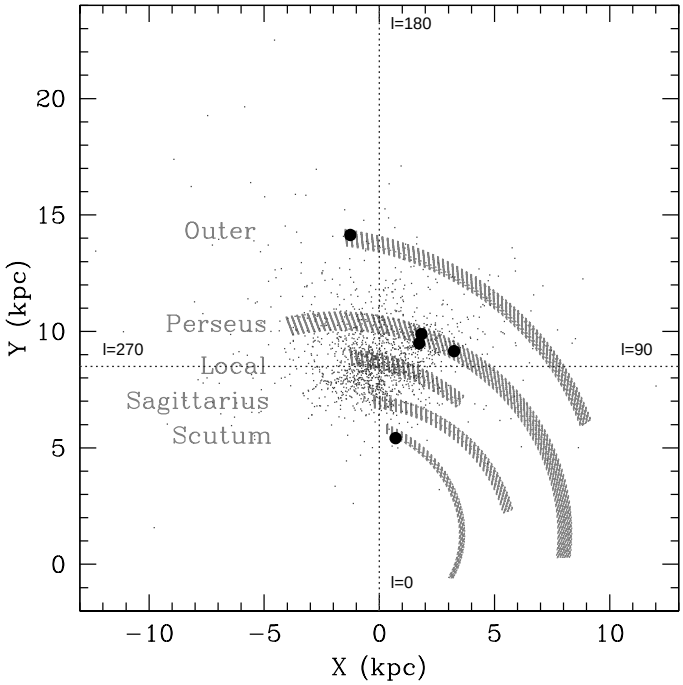

Fig. 1. Spatial distribution of the five clusters studied in this paper (filled circles) superimposed on known OCs (dots) from Dias et al. (2002). The Galaxy's spiral arm positions (dashed areas), obtained from Reid et al. (2014), have been plotted for reference. The Sun's position is shown by the intersection of the horizontal and vertical dotted lines. The location of the OCs studied here matches the position of some of the Galaxy's spiral arms (see Sect. 5.2 for discussion).

duce a breakthrough in our understanding of Galactic OCs over the coming decade.

However, most of these surveys – particularly the high-resolution spectroscopic ones – are hampered by a lack of information on cluster membership. Only a third of the approximately 2100 OCs known in our Galaxy (Dias et al. 2002)[1] have radial velocity and/or proper motion information to permit membership determination (e.g. Dias et al. 2006; Kharchenko et al. 2007). Carrera (2012, hereafter Paper I) derived radial velocities and metallicities from medium-resolution spectroscopy in four previously unstudied open clusters. With the same goal, in the current study we have acquired medium-resolution spectra for objects in the lines of sight of another five poorly studied open clusters. Our sample includes NGC 6603, one of the nearest known clusters to the Galactic centre, with a Galactocentric distance of 5.5 kpc, and Berkeley 23, one of the most distant known OCs located at around 14.2 kpc. The other three clusters studied are King 1, NGC 559, and NGC 7245, located near the Perseus spiral arm at about 10 kpc. Their spatial distribution is shown in Fig. 1, and their properties, listed in Table 1, are described in depth in Sect. 4.

This paper is organized as follows. Target selection, observations, and data reduction are described in Sect. 2; the membership selection and procedures used to determine the radial velocities and metallicities are explained in Sect. 3; the results obtained for each cluster are presented in Sect. 4; these results are discussed in Sect. 5 in the context of the trends described by OCs in the Galactic disc, and in relation to the spiral arms. Finally, our main conclusions are given in Section 6.

[1] The updated version of this catalogue can be found at `http://www.astro.iag.usp.br/ocdb/`.

2. Target selection, observations, and data reduction

Our targets were selected amongst the stars located in the expected position of the red giant branch (RGB) and the red clump (RC) in the colour–magnitude diagram of each cluster. For this purpose, we used colour–magnitude diagrams from Cignoni et al. (2011), Lata et al. (2004), Joshi et al. (2014), Sagar & Griffiths (1998), and Subramaniam & Bhatt (2007) for Berkeley 23, King 1, NGC 559, NGC 6603, and NGC 7245, respectively (Fig. 2). The *BVI* magnitudes and coordinates of the clusters studied were obtained from the WEBDA[2] database (Mermilliod 1995), except for NGC 559, for which *BV* photometry and positions were provided directly by Y. C. Joshi (private communication). The K_S magnitudes were extracted from the Two Micron All-Sky Survey (2MASS; Skrutskie et al. 2006) database[3]. In total, we observed 64 stars: 18 in NGC 559, 15 in Berkeley 23, 11 in NGC 6603, and 10 in King 1 and NGC 7245. Table 2 lists the coordinates, magnitudes, exposure times, and total signal-to-noise ratios per pixel for each target star.

Medium-resolution spectra in the region of the near-infrared Ca II triplet (CaT) at ~8500 Å were obtained using the Intermediate Dispersion Spectrograph (IDS) mounted at the Cassegrain focus of the 2.5 m Isaac Newton Telescope (INT) located at Roque de los Muchachos Observatory, Spain. Berkeley 23 was observed in service mode on 2013 January 17 and 18, and the other clusters were observed on 2014 July 18 and 19. In both cases we used the R1200R grism centred on 8500 Å and the RED+2 CCD, providing a spectral resolution of about 8000. With a few exceptions, we obtained two exposures for each target with the star shifted along the slit. In some cases, it was possible to observe another star together with the main target because it was aligned with the slit. The spectra of these additional stars were extracted and analysed in the same way as those of the main targets.

The data reduction is explained in detail in Paper I and was performed using IRAF[4] packages. Briefly, each image is overscan-subtracted, trimmed, and flatfield-corrected with the `ccdproc` tool. We did not perform bias subtraction because bias level was not constant throughout the night. Since we acquired two exposures for each target with shifts along the slit, we subtracted one from the other, obtaining a positive and a negative spectrum in the same image. In this way, we are subtracting the sky from the same physical pixel in which the star was observed, which minimizes the effect of pixel-to-pixel sensitivity variations. Of course, a time dependency remained because the two spectra had not been taken simultaneously. These sky residuals were eliminated in the following step, in which the spectrum was extracted in the traditional way using `apall` tool, and the remaining sky background was subtracted from the information on both sides of the stellar spectra. After this, each spectrum was wavelength-calibrated before the two spectra (one positive, one negative) were subtracted again to obtain the final spectrum. Finally, the spectrum was normalized by fitting a polynomial, excluding the strongest lines in the wavelength range, such as those of the calcium triplet.

[2] `http://webda.physics.muni.cz`

[3] Available at `http://irsa.ipac.caltech.edu/`.

[4] The Image Reduction and Analysis Facility, IRAF, is distributed by the National Optical Astronomy Observatories, which are operated by the Association of Universities for Research in Astronomy, Inc., under cooperative agreement with the National Science Foundation.

Table 1. Adopted cluster parameters.

Cluster	$E(B-V)$ (mag)	$(m-M)_o$ (mag)	Age (Gyr)	R_{GC} (kpc)	z (kpc)
Be 23[a]	0.33±0.08	13.8±0.1	1.1±0.2	14.2	0.55
King 1[b]	0.66±0.06	11.5±0.1	2.2±0.9	9.6	0.06
NGC 559[c]	0.76±0.06	11.8±0.1	0.4±0.2	10.0	0.03
NGC 6603[d]	0.67±0.16	12.5±0.4	0.3±0.2	5.5	−0.07
NGC 7245[e]	0.42±0.02	12.6±0.3	0.4±0.1	9.71	−0.11

[a] Average of the different values obtained by Cignoni et al. (2011). See text for details.
[b] Average of the values by Hasegawa et al. (2008) and Lata et al. (2004)
[c] Average of the values derived by Joshi et al. (2014), Maciejewski & Niedzielski (2007) and Ann & Lee (2002a)
[d] Average of the values calculated by Sagar & Griffiths (1998) and Bica et al. (1993)
[e] Average of the values obtained by Viskum et al. (1997), Kharchenko et al. (2007), Glushkova et al. (2010), and Janes & Hoq (2011)

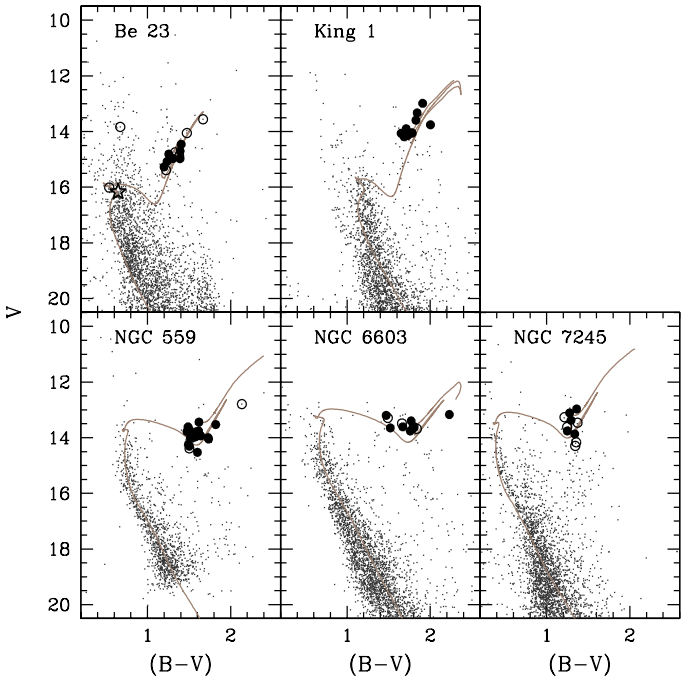

Fig. 2. Colour–magnitude diagrams of the clusters studied (small grey dots). The literature sources for the photometric data are given in the text. Filled circles are giant stars in the RGB or RC belonging to the cluster based on their radial velocities and thus used in the metallicity determination. The open star is a main sequence star in Berkeley 23 based on its radial velocity, but it has not been used in our metallicity analysis. Open circles are stars observed but classified as non-members based on their radial velocities (see Sect. 3). Isochrones derived by Pietrinferni et al. (2004) have been plotted as reference using the values listed in Table 1 and the metallicities derived in this paper. The RC position is covered by the observed stars.

3. Membership selection, radial velocity and metallicity determination

The radial velocity of each star was calculated using the `fxcor` task in IRAF, which performs a cross-correlation between the target and template spectra of known radial velocity. For Berkeley 23, we used as templates the same stars used in Paper I. For the July 2014 run, we used the stars NGC 6819 W0968 and

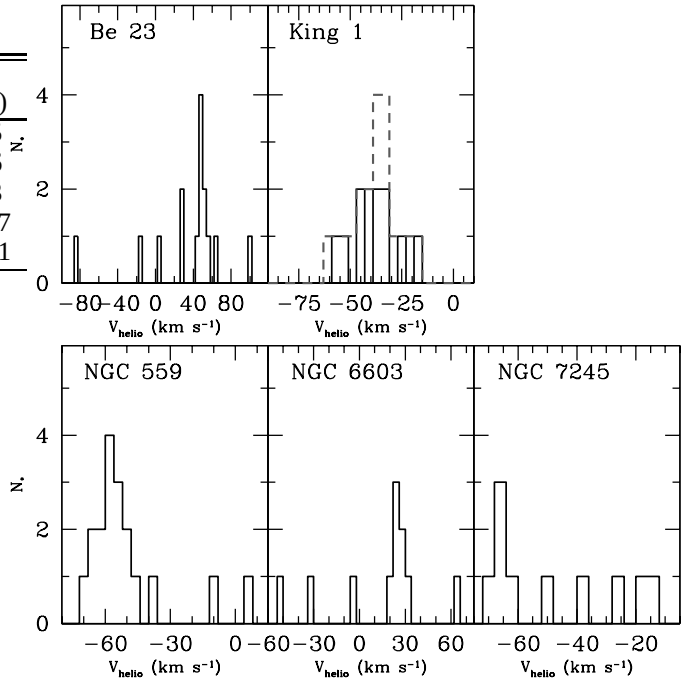

Fig. 3. Radial velocity distributions of the five OCs studied obtained using a bin of 4 km s^{-1}. In the case of King 1, the dashed line represents the histogram obtained using a bin of 8 km s^{-1}. The x-axes are not on the same scale.

NGC 6705 S5688 as templates observed on the same nights. These stars were selected because they have similar abundances and spectral types to the target stars. Moreover, their radial velocities have been accurately determined from high-resolution spectroscopy, and they have not been reported as spectroscopic binaries or radial velocity variables (Glushkova et al. 1993; Cantat-Gaudin et al. 2014). Since the radial velocities obtained using the different templates are similar within the uncertainties, the final radial velocity for each target star was obtained as the average of the velocities obtained from each template, weighted by the width of the correlation peaks. Radial velocities for each star are listed in column 9 of Table 2.

The velocity distribution of the stars observed in the area of each cluster is shown in Fig. 3 and discussed in Section 4. Cluster membership was determined from radial velocities. An iterative k-sigma clipping was used in the following way. The mean and standard deviation of the radial velocities of all the stars in the cluster area were computed. Stars with radial velocities outside $\pm 3\sigma$ were rejected. This procedure was repeated until no more stars were rejected. The final number of cluster members is listed in the last column of Table 3. The average radial velocity of each cluster, obtained as the mean of the radial velocities of all cluster members, and its standard deviations are listed in column 6 of Table 3.

Metallicities for all RC and RGB stars selected as members from their radial velocities were determined from the strengths of their CaT lines. As in Paper I, the equivalent widths of these lines were calculated using the procedure described in depth by Carrera et al. (2007). In brief, the equivalent width of each line is determined as the area between the line profile and the continuum. The line profile is determined by fitting a Gaussian plus a Lorentzian, which provides the best fit to the line core and wings. Although the spectrum was previously normalized, the continuum level is recalculated by performing a linear fit to the mean values of several continuum bandpasses defined for this purpose.

The bandpasses used to fit the line profile and to determine the continuum position are those described by Cenarro et al. (2001). The equivalent widths of each CaT line and their uncertainties, which were determined for each star, are also listed in Table 2. Finally, the CaT index, denoted ΣCa, was obtained as the sum of the equivalent widths of the three CaT lines.

The strength of the CaT lines depends not only on the chemical abundance but also on the temperature and gravity of the star. This dependence is removed because stars of the same chemical composition define a clear sequence in the luminosity–ΣCa plane when the temperature and/or gravity change. Several luminosity indicators have been used in the literature for this purpose. One of the most widely used is the magnitude of a star relative to the position of the horizontal branch (HB) in the V filter, denoted $V - V_{\rm HB}$, which also removes any dependence on distance and reddening. An alternative approach is to use the absolute magnitude in different bandpasses, such as V, I, and $K_{\rm S}$, denoted M_V, M_I, and M_K, respectively. Owing to the difficulty of defining the HB position in poorly populated clusters, we used the second approach. The absolute magnitudes of each star were obtained from the distance modulus and reddening listed in Table 1 using the extinction coefficients listed in Table 6 from Schlegel et al. (1998). The position of the member stars in each cluster in the M_V–ΣCa (left), M_I–ΣCa (centre), and M_K–ΣCa (right) planes is shown in Figure 4.

In Paper I, metallicities were calculated using the relationships derived by Carrera et al. (2007), assuming a linear relation between the CaT index and the luminosity indicators. However, Starkenburg et al. (2010) have demonstrated that this assumption is not valid, particularly for metal-poor regimes. For this reason, Carrera et al. (2013) recomputed the Carrera et al. (2007) relationships, introducing two additional terms to account for the non-linearity effects. In any case, these authors have demonstrated that both calibrations produce similar results, within ±0.2 dex, in the range of metallicities expected for open clusters. We used the most recent relationships derived by Carrera et al. (2013) to obtain the metallicities of the observed clusters. The individual values obtained for each star and bandpass are listed in Table 2. The metallicity in each bandpass is the average of all the stars in the cluster, and the associated uncertainty is the standard deviation. Finally, the metallicity of each cluster was obtained as the mean of the values obtained from each bandpass. Also, the associated uncertainties were computed as the mean of the uncertainties derived from each bandpass. This value is a better estimate of the uncertainty than the standard deviation of the metallicities calculated from each bandpass since they are not independent determinations. The mean values are listed in Table 3 and discussed below.

In this paper we have derived metallicities in both RC and RGB stars using relationships suitable for RGB stars. Du et al. (2012) have studied the behaviour of the strength of the CaT lines as a function of temperature and gravity from synthetic spectra. Their Fig. 9 predicts a slight decrease in ΣCa with temperature in the metallicity range covered by open clusters. Since RC stars are slightly hotter than RGB ones, an RC star with the same magnitude as a RGB one may have a slightly higher ΣCa. Taking NGC 559 as an example and using the relationships derived by Du et al. (2012), the maximum difference in ΣCa between RC and RGB stars is ∼0.16 Å. This implies that the metallicity of an RC star derived with the RGB relationships may be overestimated by a maximum of ∼0.07 dex, independent of the luminosity indicator used. Although systematic, this value is lower than the uncertainties of the relationships used and lower than the standard deviation of the metallicity determination of each cluster.

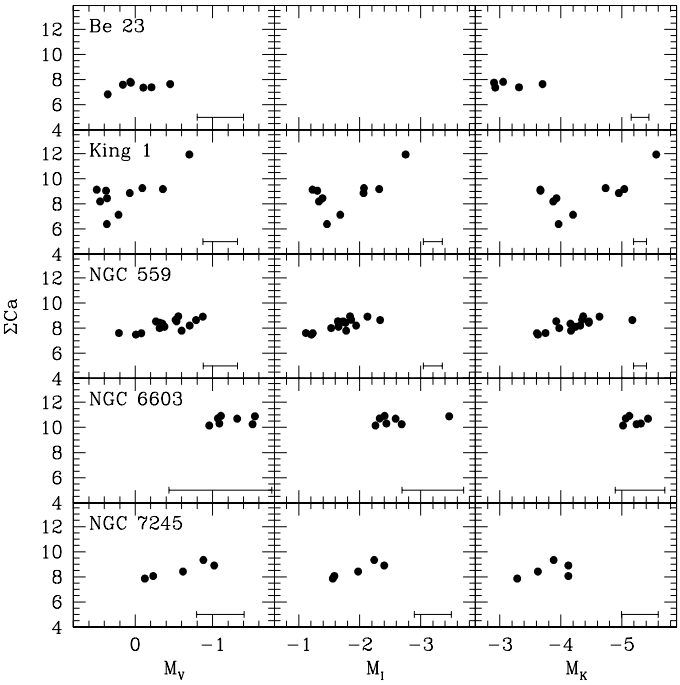

Fig. 4. Stars selected as RC or RGB members of each cluster in the M_V–ΣCa (left), M_I–ΣCa (centre), and M_K–ΣCa (right) planes. The mean sigma for each luminosity indicator is shown in bottom right corner of each panel and is mainly due to the distance modulus uncertainty. Error bars in ΣCa are smaller than the point size.

4. Cluster-by-cluster discussion

4.1. Berkeley 23

Berkeley 23 is an OC located in the third Galactic quadrant towards the Galactic anticentre. Its colour–magnitude diagram is strongly contaminated by field stars and its sequence is poorly defined. However, a broad and clumpy main sequence is still observed. Moreover, there is a mild excess of stars in the region where the RC is expected (e.g. $B - V \sim 1.2$ and $V \sim 15.0$). There are only three studies of this distant cluster in the literature. By isochrone fitting of *UBVI* colour–magnitude diagrams, Ann et al. (2002b) found an age of 790±160 Myr, a distance modulus of $(m - M)_{\rm o}$= 14.2±0.2 mag, a reddening of $E(B - V)$= 0.40±0.05 mag, and [Fe/H] = 0.07. Also, using isochrone fitting in *BVI* colour–magnitude diagrams, Hasegawa et al. (2004) derived an age of 1.8 Gyr, a distance modulus $(m-M)_{\rm o}$= 13.81 mag, a reddening $E(B-V)$= 0.30, and metallicity [Fe/H]∼ −0.7. More recently, Cignoni et al. (2011) have obtained a *BV* colour–magnitude diagram for Berkeley 23 as part of the BOCCE project. By comparing with stellar evolutionary models, they determined an age between 1.1 and 1.3 Gyr, a distance modulus $(m-M)_{\rm o}$ between 13.6 and 14.0 mag, a reddening $E(B - V)$ between 0.225 and 0.425 mag, and a metallicity between solar and half solar, i.e. [Fe/H] ∼ −0.3. The uncertainties in the parameters were caused by the difficulties in adjusting the main sequence turn-off and the RC at the same time. In general, the quantities derived by the three studies agree within the large uncertainties except for the metallicity. Here, we use the mean of the values derived by Cignoni et al. (2011) as distance modulus

Table 3. Mean cluster metallicities and radial velocities and their standard deviation. The last column lists the number of member stars.

Cluster	$[Fe/H]_V$	$[Fe/H]_I$	$[Fe/H]_K$	$\langle$ [Fe/H] $\rangle^a$	$\langle V_r \rangle^b$ (km s^{-1})	#
Be 23	−0.42±0.13		−0.43±0.13	−0.42±0.13	48.6±3.4	8[c]
King 1	+0.13±0.51	+0.00±0.52	−0.16±0.53	−0.01±0.52	−38.4±11.6	10[d]
NGC 559	−0.22±0.14	−0.18±0.14	−0.35±0.14	−0.25±0.14	−58.4±6.8	15
NGC 6603	+0.42±0.13	+0.53±0.14	+0.33±0.17	+0.43±0.15	26.0±4.3	7
NGC 7245	−0.17±0.14	−0.14±0.17	−0.15±0.24	−0.15±0.18	−65.3±3.2	5

[a] Mean of the values obtained in each bandpass. The adopted uncertainty is the mean of the uncertainties of the metallicity determination in each bandpass.
[b] Mean and standard deviation of the radial velocities of the stars selected as cluster members.
[c] Seven red giant and one main sequence stars, the latest not used in the metallicity determination.
[d] The number of stars used in our analysis. However, we cannot ensure that we have sampled real cluster members for the reasons described in Sect. 4.2

and reddening. They lie between the values derived by Ann et al. (2002b) and Hasegawa et al. (2004).

A total of fifteen stars have been observed in the Berkeley 23 area. Only eight of them have similar radial velocities defining a clear peak in the radial velocity distribution (top left panel of Fig. 3). From these eight stars we derived a mean radial velocity of $\langle V_r \rangle = 48.6 \pm 3.4$ km s^{-1}.

One of the eight stars selected as members is a main sequence star (Fig. 2) and was not used in the metallicity determination. The average metallicity of the seven giant stars is [Fe/H]= −0.42 ± 0.13 and [Fe/H] = −0.43±0.13 using V and K_S magnitudes, respectively. There are no I magnitudes in the literature. Our result is in very good agreement with the value ([Fe/H]∼ −0.3) obtained from comparison between observational and synthetic colour–magnitude diagrams by Cignoni et al. (2011). Our metallicity determination also agrees with the value ([Fe/H] ∼ −0.7) obtained by Hasegawa et al. (2004) from isochrone fitting, when taking the associate uncertainty of about ±0.3 in their method into account (corresponding to the separation in metallicity of the isochrones used).

4.2. King 1

King 1 is an old OC located in the second Galactic quadrant in the direction of the Galactic anticentre. To our knowledge, three studies in recent years have derived its physical properties from colour–magnitude diagrams. The King 1 colour–magnitude diagram shows a broad main sequence with a well-populated RC. Lata et al. (2004) used *UBVRI* photometry and isochrone fitting to obtain an age of 1.6 ± 0.4 Gyr, a distance modulus of $(m-M)_o = 11.38$ mag, and a reddening of $E(B-V) = 0.70\pm0.05$, when assuming solar metallicity. Using the same technique and *BV* wide-field photometry, Maciejewski & Niedzielski (2007) obtained an age of ∼4 Gyr, a distance modulus of $(m-M)_o = 10.17^{+0.32}_{-0.51}$ mag, and a reddening of $E(B-V) = 0.76 \pm 0.09$ mag, also assuming solar metallicity. Finally, from *VI* photometry Hasegawa et al. (2008) derived an age of 2.8 Gyr with a distance modulus $(m-M)_o = 11.57$ and reddening $E(B-V) = 0.62$ mag, when assuming solar metallicity. The values obtained by Lata et al. (2004) and Hasegawa et al. (2008) agree within the uncertainties. However, the distance modulus and age derived by Maciejewski & Niedzielski (2007) are very different from those obtained by the other two studies. For this reason, in our work we use the distance modulus and reddening obtained by averaging the values derived by Lata et al. (2004) and Hasegawa et al. (2008), as listed in Table 1, although we have investigated the impact of using the values derived by Maciejewski & Niedzielski (2007) in our results.

The ten stars observed in the King 1 area do not outline a well-defined distribution with the velocity bin of 4 km s^{-1} used to construct the velocity histograms of the other clusters (solid black histogram in middle top panel of Figure 3). Therefore, we have doubled the size to 8 km s^{-1}, but even so we find that a clear peak is not obtained. In this case none of the observed stars can be rejected from its radial velocity with the k-sigma clipping procedure used in the other clusters. The average velocity of the ten stars observed in the King 1 area is $\langle V_r \rangle = -38.4$ km s^{-1}, with a dispersion of ±11.6 km s^{-1}.

The other clusters we studied have relatively well-defined sequences in the luminosity–ΣCa planes (Fig. 4). However, the ten stars observed in King 1 are more sparsely distributed. From these stars we obtained [Fe/H] = +0.13 ± 0.51, [Fe/H] = +0.00 ± 0.52 and [Fe/H] = −0.16 ± 0.53, using V, I, and K_S, respectively. If the distance modulus and reddening derived by Maciejewski & Niedzielski (2007) are used, the metallicities obtained are higher: [Fe/H] = +0.44 ± 0.54, [Fe/H] = +0.29 ± 0.56, and [Fe/H] = +0.03 ± 0.56, using V, I, and K_S, respectively. These values seem to be too high for a cluster at the Galactocentric distance of King 1. In both cases, the derived uncertainties are twice the values obtained for the other clusters because of the high dispersion in the luminosity–ΣCa planes, as seen in Figure 4. This and the lack of a clear peak in the velocity distribution, may imply that the number of real cluster members in our sample is very small, or even zero. Therefore, both the mean radial velocity and metallicity values should be treated with caution.

4.3. NGC 559

NGC 559 is a moderately populated OC of the second Galactic quadrant located in the vicinity of the Perseus arm (Fig. 1). Its colour–magnitude diagram shows a well-populated main sequence with a diffuse but still clear RC. Several studies have been devoted to determining its properties, mainly through the use of isochrone fitting (e.g. Lindoff 1969; Jennens & Helfer 1975; Grubissich 1975; Ann & Lee 2002a; Maciejewski & Niedzielski 2007; Joshi et al. 2014). The reddening towards NGC 559 is high with a mean value of $E(B-V) = 0.76 \pm 0.06$ mag, obtained after averaging determinations from recent studies based on CCD photometry (Ann & Lee 2002a; Maciejewski & Niedzielski 2007; Joshi et al. 2014). In the same way, the mean distance modulus of NGC 559 is $(m-M)_o = 11.80 \pm 0.12$ mag. The age values determined by these studies are 225 ± 25 Myr,

obtained by Joshi et al. (2014), and 630 Myr, derived by Maciejewski & Niedzielski (2007), with a mean value of 400 ± 200 Myr. All these values were obtained assuming solar metallicity.

Only three of the 18 stars observed do not seem to be members of NGC 559 from their radial velocity. The remaining 15 stars define a clear radial velocity distribution (Fig. 3) with a mean value of $\langle V_r \rangle = -58.4 \pm 6.8$ km s^{-1}.

From these 15 stars we have derived [Fe/H] = −0.22 ± 0.14, [Fe/H] = −0.18 ± 0.14, and [Fe/H] = −0.35 ± 0.14 in the V, I, and K_S bandpasses, respectively. These results are in good agreement with the metallicity estimate obtained by Ann & Lee (2002a) from isochrone fitting ([Fe/H] ∼ −0.32). Other studies (e.g. Maciejewski & Niedzielski 2007; Joshi et al. 2014) have assumed solar metallicity.

4.4. NGC 6603

NGC 6603 is a rich OC located in the inner disc towards the Galactic centre in Sagittarius. Its colour–magnitude diagram shows features that are typical of an intermediate-age OC with the clear presence of RC stars. A few studies have been devoted to determining its physical parameters using photometry (e.g. Bica et al. 1993; Sagar & Griffiths 1998; Kharchenko et al. 2005) and integrated spectra (e.g. Santos & Bica 1993; Bica et al. 1993). These studies agree with a line-of-sight reddening between $E(B-V) = 0.50$ (Kharchenko et al. 2005) and $E(B-V) = 0.56$ (Sagar & Griffiths 1998) in the direction of NGC 6603 and an internal reddening of $E(B-V) = 0.29$ mag (Bica et al. 1993). The distance modulus is constrained between $(m-M)_o = 12.16$ (Sagar & Griffiths 1998) and $(m-M)_o = 12.78$ (Bica et al. 1993) with a mean value of $(m-M)_o = 12.41 \pm 0.32$ mag. The age determined for NGC 6603 is between 200 ± 100 Myr (Bica et al. 1993) and 500 Myr (Sagar & Griffiths 1998), although Kharchenko et al. (2005) assigned an age of 60 Myr to this cluster. To our knowledge, NGC 6603 is the only cluster in our sample in which spectra of individual stars have been previously acquired. Frinchaboy & Majewski (2008) acquired medium-resolution ($R \sim 15\,000$) spectra for 55 stars in NGC 6603. From proper motions and radial velocities, they concluded that only four of them were NGC 6603 members with a mean radial velocity of $\langle V_r \rangle = 21.34 \pm 0.92$ km s^{-1}.

Of the 11 stars observed in our sample, only seven are cluster members, the other four having discordant radial velocities. We derived a mean radial velocity of $\langle V_r \rangle = 26.0 \pm 4.3$ km s^{-1}. This value agrees, within the uncertainties, with the mean radial velocity found by Frinchaboy & Majewski (2008). A direct comparison with their results is not possible because there are no stars in common.

For NGC 6603 we derived a mean metallicity of [Fe/H] = +0.42 ± 0.13, +0.53 ± 0.14, and +0.33 ± 0.17 from V, I, and K_S magnitudes, respectively. This places NGC 6603 within the most metal-rich OCs known. Of course, this result has to be confirmed by high-resolution spectroscopy. All previous studies of this cluster have assumed a solar metallicity (e.g. Sagar & Griffiths 1998; Kharchenko et al. 2005), which does not seem to be the case.

4.5. NGC 7245

NGC 7245 is a sparse cluster located in the second Galactic quadrant. Its colour–magnitude diagram shows a well-defined main sequence with a sparse concentration of stars in the expected position of the RC (e.g. $B-V \sim 1.3$ and $V \sim 13.6$). One of the first photometric studies in this cluster Yilmaz (1970) using the *RGU* system found a distance modulus $(m-M)_o = 11.42$ and reddening $E(B-V) \sim 0.60$ mag. More recently, and on the basis of *BV* Johnson CCD photometry and isochrone fitting, Viskum et al. (1997) derived an age of 320 Myr, distance modulus $(m-M)_o = 12.23 \pm 0.15$, and reddening $E(B-V) = 0.40 \pm 0.02$ mag, assuming solar metallicity. From *UBV* CCD photometry Kharchenko et al. (2007) find an age of 400 Myr, distance modulus $(m-M)_o = 12.9 \pm 0.2$ mag, and reddening $E(B-V) = 0.45 \pm 0.02$ mag, assuming solar metallicity. Glushkova et al. (2010) used BVR_cI_c photometry to estimate an age of 320 ± 40 Myr with a distance modulus $(m-M)_o = 12.65 \pm 0.13$ and reddening $E(B-V) = 0.42 \pm 0.03$ mag, assuming solar metallicity. Finally, Janes & Hoq (2011) derived an age of 445 Myr with a distance modulus $(m-M)_o = 12.7$ and reddening $E(B-V) = 0.45$ mag from *VI* photometry, also assuming solar metallicity. Since all studies based on CCD photometry produce relatively similar results within the uncertainties, we used as reddening and distance modulus the average of the values obtained by Viskum et al. (1997), Kharchenko et al. (2007), Glushkova et al. (2010), and Janes & Hoq (2011), listed in Table 1.

Five of the ten stars observed in NGC 7245 define a clear peak in the velocity distribution (bottom right panel of Fig. 3). The remaining stars have discordant radial velocities. The mean radial velocity of the five stars selected as members is $\langle V_r \rangle = -65.3 \pm 3.2$ km s^{-1}.

From the NGC 7245 members, we obtained an average metallicity of [Fe/H] = −0.17 ± 0.14, [Fe/H] = −0.14 ± 0.17, and [Fe/H] = −0.15 ± 0.24 using V, I, and K_S, respectively. There are no metallicity determinations of this cluster in the literature, and all studies using isochrone fitting have assumed a solar content.

5. Discussion

5.1. Comparison with trends in the Galactic disc

Observed trends described by OCs in the Galactic disc (e.g. metallicity with Galactocentric distance, R_{GC}, vertical distance to the Galactic plane, $|z|$, and age) indicate that the chemical composition of OCs is determined mainly by their location in the disc and not by the moment when they were formed (e.g. Carrera & Pancino 2011). It is therefore helpful to compare the clusters studied here with the trends described by the bulk of OCs in order to check that they share features. This comparison is even more important in our case because our sample includes clusters in poorly sampled regions of the disc, such as the innermost and outermost areas. To do this comparison we used the compilation of clusters obtained by Carrera & Pancino (2011). Briefly, their sample includes chemical abundances available in the literature derived from high-resolution spectroscopy ($R \geq 18\,000$). We refer the reader to that paper for more details. The run of metallicity with R_{GC}, age, and $|z|$ for this sample has been plotted in the top, middle, and bottom panels of Fig. 5, respectively. The top panel shows linear fits to the sample, when assuming a change in the slope at $R_{GC} \sim 12.5$ kpc, the linear fit to the whole sample. It also plots clusters in the inner 10 kpc and from there outwards in the three panels.

The five clusters studied here closely follow the trends observed in the Galactic disc. Berkeley 23 has a similar metallicity to other OCs located at the same Galactocentric distance. NGC 6603 is located even farther in than the innermost OCs in the Carrera & Pancino (2011) sample. If the high metallicity obtained here for this cluster is confirmed by high-resolution data, this may imply that the metallicity gradient in the inner

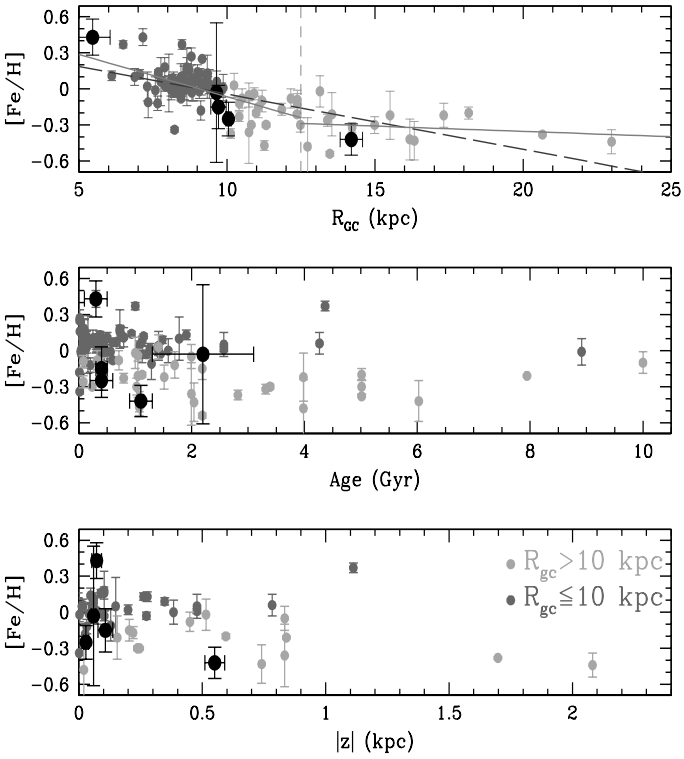

Fig. 5. Gradient in [Fe/H] as a function of R_{GC} (top), age (middle), and $|z|$ (bottom) of the OCs in the Carrera & Pancino (2011) compilation. For the clusters studied here, we have used the weighted mean of the values obtained in the three bands listed in column 5 of Table 3. Dark and light grey points are clusters inside and outside radial distances of 10 kpc, respectively. Black points are the clusters studied in this paper. Solid lines in the top panel represent two separate linear fits obtained by Carrera & Pancino (2011) for OC inside and outside 12.5 kpc. The dashed line is the fit obtained by the same authors using all open clusters.

disc is even steeper than previously thought. The three other OCs match the observed trends even when considering the large uncertainties in the metallicity determination of King 1. NGC 559, NGC 7245, and King 1 are located almost in the Galactic plane, $|z| \leq 120$ pc, with metallicities similar to other coeval OCs located at the same vertical distances. Only Berkeley 23 has a considerable vertical distance from the Galactic plane, in agreement with other clusters located at similar Galactocentric distances. All of them match the age–metallicity distribution described by most open clusters.

Finally, the high metallicity of NGC 6603 seems to place this cluster outside the age and distance from the plane distributions defined by most of the open clusters. There are at least three known OCs with [Fe/H] ≥ 0.3. These are NGC 6253, NGC 6583 and NGC 6791. Two of them (NGC 6253 and NGC 6583) are located at similar distances from the Galactic plane, although they are situated at slightly different Galactocentric distances from NGC 6603. Moreover, NGC 6253 has a similar age to NGC 6603, whereas NGC 6583 is slightly older. Only NGC 6791 differs from the other three very metal-rich OCs: it is older, more distant, and is located more than 1 kpc above the Galactic plane.

Summarizing, the values derived for the five clusters studied here match the metallicities of other OCs with similar ages and locations in the Galactic plane.

5.2. Relation to spiral arms

From Fig. 1 it is noteworthy that King 1, NGC 559, and NGC 7245 are located in the Perseus spiral arm and Berkeley 23 in the outer spiral arm. NGC 6603 is located near the Scutum arm. It is therefore interesting to investigate the relation of these clusters with such arms.

The first three columns of Table 4 list the heliocentric radial velocities induced by differential Galactic rotation and the peculiar motion of the Sun with respect to the local standard of rest (LSR) projected onto the line of sight of each cluster, V_r^{GC} using the Sun's location and Galactic rotation computed or adopted by Reid et al. (2014), Antoja et al. (2011), and Sofue et al. (2009). The peculiar motion of the Sun has been adopted as $U_\odot = 10.7$, $V_\odot = 15.6$, and $W_\odot = 7.0$ km s^{-1} (Reid et al. 2014). The error margins of V_r^{GC} were computed using the $\pm\sigma_{(m-M)_o}$ values listed in Table 1. For NGC 6603, the distance modulus uncertainty introduces more variation than the difference among adopted Galactic parameters. For King 1, NGC 559, and NGC 7245, the three clusters in the Perseus arm, all results are marginally compatible. Finally, for Berkeley 23, the difference in Galactic parameters is larger than the difference due to the distance modulus uncertainty. Adopting the same values as Antoja et al. (2011), which results in intermediate values for V_r^{GC}, the peculiar radial velocities of the clusters with respect to their LSR were computed as $V_r^{pec} = \langle V_r \rangle - V_r^{GC}$. The values are also listed in Table 4 (last column). The errors are computed as $\sqrt{\sigma^2_{\langle V_r \rangle} + \sigma^2_{V_r^{GC}}}$. Of the three clusters located in the Perseus arm, NGC 559 and NGC 7245 have the same age and V_r^{pec}, and they have compatible [Fe/H] values. Taken together, these values may indicate a relationship in the formation of these open clusters. The peculiar radial velocities also roughly agree with the values found by Reid et al. (2014) for a set of high-mass star-forming regions in the same arms.

Table 4. Heliocentric radial velocities computed using three different Sun's locations and Galactic rotations and the peculiar radial with respect to the local standard of rest (LSR). Units are km s^{-1}.

Cluster	$V_r^{GC(1)}$	$V_r^{GC(2)}$	$V_r^{GC(3)}$	V_r^{pec}
Scutum:				
NGC 6603	$17.0^{+10.7}_{-7.3}$	$13.7^{+9.4}_{-6.5}$	$13.6^{+9.8}_{-6.6}$	$12.3^{+10.3}_{-7.8}$
Perseus:				
King 1	$-33.8^{+1.1}_{-1.2}$	$-31.3^{+1.0}_{-1.1}$	$-30.5^{+1.0}_{-1.0}$	$-7.1^{+11.6}_{-11.6}$
NGC 559	$-36.3^{+1.3}_{-1.3}$	$-33.3^{+1.1}_{-1.2}$	$-32.3^{+1.1}_{-1.1}$	$-25.1^{+6.9}_{-6.9}$
NGC 7245	$-43.2^{+4.7}_{-5.5}$	$-40.0^{+4.2}_{-5.0}$	$-39.5^{+4.1}_{-4.8}$	$-25.3^{+5.3}_{-5.9}$
Outer:				
Berkeley 23	$34.3^{+0.6}_{-0.6}$	$32.3^{+0.5}_{-0.5}$	$31.2^{+0.5}_{-0.5}$	$16.3^{+3.4}_{-3.4}$

(1): $\Theta_0 = 240$ km s^{-1}, $R_0 = 8.34$ kpc; Reid et al. (2014)
(2): $\Theta_0 = 220$ km s^{-1}, $R_0 = 8.50$ kpc; Antoja et al. (2011)
(3): $\Theta_0 = 200$ km s^{-1}, $R_0 = 8.00$ kpc; Sofue et al. (2009)
$d\Theta/dR = -0.2$ km s^{-1} kpc^{-1}; Reid et al. (2014)

Mean radial velocities were combined with proper motions to derive full spatial velocities. Mean proper motions were taken from Dias et al. (2014) and are listed in Table 5. These proper motions are based on the UCAC4 catalogue (Zacharias et al. 2013). A comparison between UCAC4 and PPMXL (Roeser et al. 2010) proper motions for the stars in common in the entire cluster area yields large differences, as large as the proper mo-

tions themselves. For our radial velocity members, there is no coherence among proper motions, either in the UCAC4 or in the PPMXL, or between the UCAC4 and the PPMXL. In spite of these uncertainties, we computed the non-circular velocity components (U_s, V_s, W_s), which are also listed in Table 5. To estimate the uncertainties, we performed a classical Markov chain Monte Carlo simulation for each cluster with 10 000 random realizations, accounting for the uncertainties in distance modulus, proper motions, and radial velocity. The mean values of the 10 000 cases are taken as the estimated velocity components and their standard deviation as the estimation of the uncertainties. These uncertainties reflect the large uncertainties in the proper motions and prevent us from deriving kinematics in the arms.

6. Conclusions

We have obtained medium-resolution spectra ($R \sim 8000$) in the near-infrared CaT region (~8 500 Å) for 64 stars in the line of sight towards five OCs: Berkeley 23, King 1, NGC 559, NGC 6603, and NGC 7245. To our knowledge, these are the first radial velocity and metallicity determinations from spectroscopy available in the literature, except for NGC 6603, where radial velocities of four members were previously measured by Frinchaboy & Majewski (2008). Our main results may be summarized as follows:

- Of the 15 stars analysed in Berkeley 23, only eight were determined from their radial velocities to be members, with one of them a main sequence star. We derived a mean radial velocity of $\langle V_r \rangle = 48.6 \pm 3.4$ km s^{-1} from these eight members. Excluding the main sequence star, we derived [Fe/H] $= -0.42 \pm 0.13$.
- Ten stars were sampled in the King 1 area. However, they do not define a clear radial velocity distribution. Moreover, they do not trace a clear sequence in the magnitude-ΣCa planes for any of the three luminosity indicators used. In any case, we derived a mean radial velocity and metallicity for this cluster in the same way as for the others, with the uncertainties in these determinations accounting for the observed dispersion. We obtained an average radial velocity of $\langle V_r \rangle = -38.4 \pm 11.6$ km s^{-1} and a mean metallicity of [Fe/H] $= +0.01 \pm 0.52$. These results should be treated with caution because we cannot ensure that we have sampled real cluster members.
- For NGC 559, we derived a mean radial velocity of $\langle V_r \rangle = -58.4 \pm 6.8$ km s^{-1} from 15 of the 18 stars observed. The metallicity obtained is [Fe/H] $= -0.25 \pm 0.14$.
- For NGC 6603, one of the closest known OCs to the Galactic centre, we determined an average radial velocity of $\langle V_r \rangle = 26.0 \pm 4.3$ km s^{-1} from 7 of the 11 stars observed. The metallicity derived ([Fe/H] $= +0.43 \pm 0.15$) places this cluster within the most metal-rich OCs known.
- In the case of NGC 7245, the mean redial velocity, $\langle V_r \rangle = -65.3 \pm 3.2$ km s^{-1}, was obtained from five of the ten stars observed. We obtained an average metallicity of [Fe/H] $= -0.15 \pm 0.18$.

We compared the properties derived here for the five clusters in our sample with the trends observed for other OCs in the Galactic disc. All the clusters studied follow the trend described by other coeval OCs located at similar Galactocentric distances very well. NGC 6603 may play an important role in our understanding of the trends observed in the Galactic disc. If the high metallicity derived here is confirmed by high-resolution spectroscopy, the metallicity gradient in the inner disc could be even steeper than previously thought.

The mean radial velocities $\langle V_r \rangle$ were used to derive the peculiar radial velocity of the clusters with respect to their LSR V_r^{pec}. These values are compatible with those of high-mass star-forming regions in the same arms (Reid et al. 2014). NGC 559 and NGC 7245 in the Perseus arm have the same age and the same V_r^{pec}, and have compatible [Fe/H], too. These features, taken together, may indicate some kind of relationship in their formation.

We also derived full spatial velocities for the clusters by combining our mean radial velocities with mean proper motions from the literature. However, the uncertainty in the proper motions prevents any further study of the kinematics or any meaningful comparison with the velocities of the high-mass star-forming regions mentioned above.

Acknowledgements. We acknowledge the anonymous referee for their useful comments which have contributed to clarify the presentation of our results. This research made use of the WEBDA database, operated at the Department of Theoretical Physics and Astrophysics of the Masaryk University, and the SIMBAD database, operated at the CDS, Strasbourg, France. This publication makes use of data products from the Two Micron All Sky Survey, which is a joint project of the University of Massachusetts and the Infrared Processing and Analysis Center/California Institute of Technology, funded by the National Aeronautics and Space Administration and the National Science Foundation. This research was supported by the MINECO (Spain's Ministry of Economy and Competitiveness) - FEDER through grants AYA2013-42781P, AYA2012-39551-C02-01, AYA2010-16717, AYA2008-01839 and ESP2013-48318-C2-1-R.

References

Anguiano, B., Freeman, K., Bland-Hawthorn, J., et al. 2014, IAU Symposium, 298, 322
Ann, H. B., & Lee, S. H. 2002a, Journal of Korean Astronomical Society, 35, 29
Ann, H. B., Lee, S. H., Sung, H., et al. 2002b, AJ, 123, 905
Antoja, T., Figueras, F., Romero-Gómez, M., et al. 2011, MNRAS, 418, 1423
Bica, E., Ortolani, S., & Barbuy, B. 1993, A&A, 270, 117
Bragaglia, A., & Tosi, M. 2006, AJ, 131, 1544
Cantat-Gaudin, T., Vallenari, A., Zaggia, S., et al. 2014, A&A, 569, AA17
Carrera, R., Casamiquela, L., Balaguer-Núñez, L., et al. 2014, Highlights of Spanish Astrophysics VIII arXiv:1412.3509
Carrera, R., Gallart, C., Pancino, E., & Zinn, R. 2007, AJ, 134, 1298
Carrera, R., Pancino, E., Gallart, C., & del Pino, A. 2013, MNRAS, 434, 1681
Carrera, R., & Pancino, E. 2011, A&A, 535, A30
Carrera, R. 2012, A&A, 544, A109
Cenarro, A. J., Cardiel, N., Gorgas, J., et al. 2001, MNRAS, 326, 959
Cignoni, M., Beccari, G., Bragaglia, A., & Tosi, M. 2011, MNRAS, 416, 1077
Conrad, C., Scholz, R.-D., Kharchenko, N. V., et al. 2014, A&A, 562, A54
Dias, W. S., Alessi, B. S., Moitinho, A., & Lépine, J. R. D. 2002, A&A, 389, 871
Dias, W. S., Assafin, M., Flório, V., Alessi, B. S., & Líbero, V. 2006, A&A, 446, 949
Dias, W. S., Monteiro, H., Caetano, T. C., et al. 2014, A&A, 564, AA79
Donati, P., Cantat Gaudin, T., Bragaglia, A., et al. 2014, A&A, 561, A94
Du, W., Luo, A. L., & Zhao, Y. H. 2012, AJ, 143, 44
Frinchaboy, P. M., & Majewski, S. R. 2008, AJ, 136, 118
Frinchaboy, P. M., Thompson, B., Jackson, K. M., et al. 2013, ApJ, 777, L1
Glushkova, E. V., Kulagin, Y. V., & Rastorguev, A. S. 1993, Astronomy Letters, 19, 232
Glushkova, E. V., Zabolotskikh, M. V., Koposov, S. E., et al. 2010, Astronomy Letters, 36, 14
Grubissich, C. 1975, A&AS, 21, 99
Hasegawa, T., Malasan, H. L., Kawakita, H., et al. 2004, PASJ, 56, 295
Hasegawa, T., Sakamoto, T., & Malasan, H. L. 2008, PASJ, 60, 1267
Janes, K. A., & Hoq, S. 2011, AJ, 141, 92
Jennens, P. A., & Helfer, H. L. 1975, MNRAS, 172, 681
Joshi, Y. C., Balona, L. A., Joshi, S., & Kumar, B. 2014, MNRAS, 437, 804
Kharchenko, N. V., Piskunov, A. E., Röser, S., Schilbach, E., & Scholz, R.-D. 2005, A&A, 438, 1163
Kharchenko, N. V., Scholz, R.-D., Piskunov, A. E., Röser, S., & Schilbach, E. 2007, Astronomische Nachrichten, 328, 889
Lata, S., Mohan, V., & Sagar, R. 2004, Bulletin of the Astronomical Society of India, 32, 371

Table 5. Mean proper motions and their errors from Dias et al. (2014) for our cluster sample. U_s, V_s, and W_s are the components of the non-circular velocity at the position of each cluster. They are computed from proper motions and radial velocities using the values for the motion of the Sun with respect to the LSR from Reid et al. (2014) and Galactic rotation as $\Theta_0 = 220$ km s^{-1}, $R_0 = 8.50$ kpc, and $d\Theta/dR = -0.2$ km s^{-1} kpc^{-1}.

Cluster	$\mu_\alpha \cos\delta$ (mas yr^{-1})	μ_δ (mas yr^{-1})	U_s (km s^{-1})	V_s (km s^{-1})	W_s (km s^{-1})
Scutum:					
NGC 6603	1.06±4.06	−0.74±5.12	4.68±26.75	22.11± 72.15	−13.46±69.58
Perseus:					
King 1	−2.43±2.59	1.02±1.50	34.91±44.01	17.43± 36.75	21.55±15.70
NGC 559	−4.58±2.95	1.41±1.46	86.82±47.90	58.09± 52.77	5.04±18.88
NGC 7245	−1.98±3.58	−1.76±3.19	16.99±73.88	−18.66± 45.73	16.73±69.93
Outer:					
Berkeley 23	2.65±2.10	−7.32±4.68	9.55±13.39	−204.98±116.58	−10.75±78.99

Lee, Y. S., Beers, T. C., Sivarani, T., et al. 2008, AJ, 136, 2050
Lindegren, L. 2005, The Three-Dimensional Universe with Gaia, 576, 29
Lindoff, U. 1969, Arkiv for Astronomi, 5, 221
Maciejewski, G., & Niedzielski, A. 2007, A&A, 467, 1065
Mermilliod, J.-C. 1995, Information & On-Line Data in Astronomy, 203, 127
Mignard, F. 2005, The Three-Dimensional Universe with Gaia, 576, 5
Pancino, E., Carrera, R., Rossetti, E., & Gallart, C. 2010, A&A, 511, AA56
Perryman, M. A. C., de Boer, K. S., Gilmore, G., et al. 2001, A&A, 369, 339
Pietrinferni, A., Cassisi, S., Salaris, M., & Castelli, F. 2004, ApJ, 612, 168
Reid, M. J., Menten, K. M., Brunthaler, A., et al. 2014, ApJ, 783, 130
Roeser, S., Demleitner, M., & Schilbach, E. 2010, AJ, 139, 2440
Sagar, R., & Griffiths, W. K. 1998, MNRAS, 299, 1
Santos, J. F. C., Jr., & Bica, E. 1993, MNRAS, 260, 915
Schlegel, D. J., Finkbeiner, D. P., & Davis, M. 1998, ApJ, 500, 525
Sofue, Y., Honma, M., & Omodaka, T. 2009, PASJ, 61, 227
Subramaniam, A., & Bhatt, B. C. 2007, MNRAS, 377, 829
Starkenburg, E., Hill, V., Tolstoy, E., et al. 2010, A&A, 513, A34
Skrutskie, M. F., Cutri, R. M., Stiening, R., et al. 2006, AJ, 131, 1163
Viskum, M., Hernandez, M. M., Belmonte, J. A., & Frandsen, S. 1997, A&A, 328, 158
Yilmaz, F. 1970, A&A, 8, 213
Zacharias, N., Finch, C. T., Girard, T. M., et al. 2013, AJ, 145, 44

Table 2. Observing logs and program star information.

Cluster	Star[a]	α_{2000} (hrs)	δ_{2000} (deg)	V (mag)	B (mag)	I (mag)	K_S (mag)	V_r (km s^{-1})	EW$_{8498}$ (Å)	EW$_{8442}$ (Å)	EW$_{8662}$ (Å)	[Fe/H]$_V$	[Fe/H]$_I$	[Fe/H]$_K$	t$_{exp}$ (sec)	S/N per pixel	Date	Note
Be23	W112	06:33:15.9	+20:31:04.1	14.977	16.368		11.736	50.84±3.95	1.76±0.05	3.64±0.07	2.41±0.08	-0.25±0.10	21.73±3.09	-0.29±0.06	2x700	32	17012013	0
	W104	06:33:15.2	+20:32:05.8	14.968	16.275		11.886	46.82±3.44	1.65±0.05	3.83±0.09	2.27±0.06	-0.28±0.10	21.61±3.07	-0.28±0.06	2x700	32	17012013	0
	W124	06:33:18.4	+20:32:06.6	15.268	16.467		12.394	47.65±4.05	1.20±0.07	3.35±0.08	2.27±0.06	-0.58±0.10	19.93±2.90	-0.59±0.06	2x700	29	17012013	0
	W159	06:33:19.9	+20:29:28.0	16.166	16.813			51.47±10.91							2x700	9	17012013	2
	W089	06:33:22.3	+20:32:51.9	14.808	16.064		11.866	54.92±3.25	1.30±0.05	3.19±0.06	2.87±0.07	-0.49±0.10	20.90±3.00	-0.46±0.06	2x700	31	17012013	0
	W079	06:33:09.2	+20:27:21.3	14.460	15.865		11.090	46.39±4.76	1.45±0.05	3.54±0.06	2.65±0.05	-0.48±0.10	21.40±3.05	-0.51±0.05	2x650	39	18012013	0
	W092	06:33:00.2	+20:31:44.1	14.702	16.095		11.476	44.89±4.64	1.53±0.07	3.30±0.08	2.56±0.09	-0.51±0.10	20.94±3.00	-0.54±0.06	2x650	26	18012013	0
	W106	06:33:18.4	+20:33:31.6	15.072	16.309		12.191	46.24±5.20	1.44±0.09	3.78±0.07	2.38±0.08	-0.31±0.10	21.32±3.04	-0.29±0.06	2x700	23	18012013	0
	W135	06:33:17.0	+20:32:06.3	16.011	16.551		14.347	99.82±11.92							2x700	17	17012013	1
	W102	06:33:19.2	+20:31:34.5	14.881	16.262		11.666	26.07±3.11							2x700	34	17012013	1
	W141	06:33:20.1	+20:31:17.9	15.383	16.607		12.506	26.33±4.47							2x700	25	17012013	1
	W091	06:33:21.8	+20:29:49.8	14.747	16.081		11.724	4.96±3.51							2x700	24	17012013	1
	W025	06:33:17.6	+20:26:06.5	13.832	14.505		12.019	-17.84±3.86							2x700	22	17012013	1
	W038	06:33:20.6	+20:26:23.5	13.557	15.226		9.911	-85.37±5.22							2x700	67	17012013	1
	W059	06:33:01.9	+20:35:33.5	14.052	15.526		10.720	62.36±5.14							2x600	41	18012013	1
King1	W0117	00:21:50.8	+64:30:13.6	14.062	15.712	11.901	9.773	-26.87±2.03	1.49±0.05	4.32±0.04	3.23±0.05	0.36±0.08	0.26±0.06	0.12±0.04	2x300	44	19072014	3
	W0296	00:22:47.5	+64:28:54.1	12.985	14.894	10.451	7.874	-46.94±1.98	1.97±0.03	5.32±0.03	4.64±0.04	1.16±0.09	1.04±0.06	0.89±0.04	2x150	60	19072014	3
	W0405	00:22:43.5	+64:28:18.8	13.901	15.612	11.524	9.240	-31.64±2.34	1.18±0.04	3.43±0.05	2.52±0.05	-0.49±0.07	-0.66±0.05	-0.85±0.04	2x300	46	19072014	3
	W0971	00:22:22.5	+64:25:07.9	14.183	15.869	11.979	9.777	-35.58±3.01	1.72±0.04	4.28±0.04	3.13±0.04	0.44±0.08	0.32±0.06	0.16±0.04	2x300	43	19072014	3
	W1092	00:22:18.1	+64:24:39.1	13.327	15.17	10.885	8.398	-34.13±1.51	1.63±0.03	4.44±0.03	3.11±0.04	0.17±0.08	0.04±0.05	-0.15±0.04	2x250	62	19072014	3
	W1280	00:22:09.0	+64:23:46.8	13.756	15.759	11.141	8.488	-37.36±1.88	1.45±0.03	4.24±0.03	3.17±0.03	0.19±0.07	-0.02±0.05	-0.27±0.04	2x250	65	19072014	3
	W1775	00:21:50.7	+64:21:31.5	14.052	15.835	11.742	9.477	-51.40±2.23	0.75±0.04	3.18±0.06	2.46±0.09	-0.76±0.08	-0.92±0.06	-1.13±0.05	2x300	47	19072014	3
	W2104	00:22:34.2	+64:19:44.9	13.593	15.421	11.135	8.705	-56.65±2.42	1.76±0.03	4.45±0.02	3.04±0.04	0.29±0.08	0.14±0.05	-0.05±0.04	2x300	58	19072014	3
	W2282	00:21:35.5	+64:19:03.1	14.139	15.867	11.874	9.565	-45.21±1.81	1.39±0.04	3.95±0.05	2.86±0.04	0.03±0.08	-0.11±0.06	-0.31±0.04	2x300	50	19072014	3
	W2410	00:21:27.2	+64:18:27.4	14.049	15.826	11.815	9.512	-18.53±1.88	1.46±0.04	4.22±0.04	2.76±0.04	0.11±0.08	-0.02±0.05	-0.21±0.04	2x300	41	19072014	3
NGC559	J0010	01:29:36.7	+63:22:08.0	12.792	14.927	10.065	7.215	-11.13±1.70							2x300	80	18072014	1
	J0018	01:29:31.1	+63:18:12.5	13.442	15.061	11.514	9.400	-65.48±2.51	1.83±0.05	4.21±0.05	2.88±0.05	-0.10±0.08	-0.01±0.06	-0.17±0.04	2x300	50	18072014	0
	J0020	01:29:46.0	+63:19:27.0	13.529	15.350	11.306	8.861	-61.91±1.62	1.44±0.04	4.42±0.03	2.78±0.04	-0.18±0.07	-0.19±0.05	-0.41±0.04	2x300	50	18072014	0
	J0025	01:28:41.2	+63:20:47.8	13.612	15.100	11.700	9.716	-63.63±3.14	1.21±0.04	4.00±0.04	3.00±0.03	-0.33±0.07	-0.26±0.05	-0.40±0.04	2x300	46	19072014	0
	J0027	01:29:45.6	+63:18:42.2	13.716	15.218	11.864	9.868	-55.26±2.07	1.36±0.04	3.79±0.05	2.65±0.05	-0.46±0.07	-0.39±0.05	-0.54±0.04	2x300	43	18072014	0
	J0030	01:29:20.9	+63:17:36.4	13.758	15.372	11.800	9.667	-51.97±2.54	1.55±0.06	4.29±0.09	3.11±0.07	0.01±0.09	0.07±0.07	-0.09±0.06	2x300	32	18072014	0
	J0033	01:30:08.0	+63:18:33.8	13.781	15.256	11.999	10.110	-57.90±2.54	1.38±0.05	4.35±0.10	2.81±0.06	-0.14±0.09	-0.04±0.07	-0.16±0.06	2x300	33	18072014	0
	J0034	01:29:59.1	+63:22:37.8	13.794	15.380	11.780	9.687	-70.71±2.24	1.49±0.04	4.29±0.06	2.89±0.05	-0.08±0.08	-0.05±0.06	-0.21±0.05	2x300	49	18072014	0
	J0038	01:29:29.3	+63:18:05.6	13.937	15.578	11.990	9.792	-66.61±1.85	1.51±0.03	3.94±0.03	2.67±0.04	-0.26±0.07	-0.23±0.05	-0.42±0.04	2x300	62	18072014	0
	J0040	01:29:41.5	+63:17:55.1	13.965	15.544	11.987	9.876	-59.81±2.06	1.57±0.02	4.08±0.04	2.71±0.06	-0.16±0.08	-0.13±0.06	-0.30±0.04	2x300	68	19072014	0
	J0041	01:29:58.2	+63:18:21.1	13.972	15.518	12.058	9.991	5.16±2.47							2x300	42	18072014	1
	J0043	01:29:32.2	+63:18:45.7	14.000	15.517	12.110	10.060	-59.41±2.45	1.42±0.03	3.86±0.04	2.73±0.04	-0.29±0.07	-0.24±0.05	-0.41±0.04	2x300	57	19072014	0
	J0044	01:29:34.2	+63:19:19.6	14.001	15.730	11.875	9.575	-55.86±2.32	1.41±0.02	3.94±0.03	3.09±0.03	-0.11±0.07	-0.12±0.05	-0.34±0.04	2x300	79	18072014	0
	J0049	01:29:42.0	+63:16:52.4	14.049	15.784	11.914	9.575	-57.81±2.04	1.62±0.03	4.15±0.03	2.76±0.04	-0.06±0.07	-0.07±0.05	-0.29±0.04	2x300	57	19072014	0
	J0061	01:29:15.3	+63:18:07.3	14.236	15.728	12.411	10.427	-51.09±2.13	1.43±0.04	3.46±0.05	2.71±0.04	-0.38±0.07	-0.34±0.05	-0.51±0.04	2x300	46	18072014	0
	J0067	01:29:34.2	+63:20:29.9	14.307	15.810	12.434	10.410	-54.68±2.95	1.32±0.06	3.57±0.06	2.60±0.08	-0.41±0.08	-0.38±0.06	-0.56±0.05	2x300	32	18072014	0
	J0070	01:30:04.8	+63:19:26.3	14.380	15.884	12.490	10.494	-37.12±2.72							2x300	32	18072014	1
	J0082	01:29:48.6	+63:15:29.1	14.527	16.128	12.525	10.286	-44.17±4.55	1.42±0.03	3.56±0.05	2.63±0.05	-0.29±0.07	-0.31±0.06	-0.54±3.05	2x300	36	18072014	0
NGC6603	W1653	18:18:31.5	-18:25:48.0	13.62	15.42	11.72	8.976	-32.44±1.78							2x400	86	18072014	1
	W1727	18:18:30.7	-18:24:24.4	13.29	14.78	11.72	9.351	-5.40±2.42							2x350	62	19072014	1
	W1755	18:18:30.5	-18:25:04.0	13.68	15.52	11.86	8.884	63.55±2.10							2x400	97	18072014	1
	W1997	18:18:28.5	-18:24:57.0	13.61	15.28	11.81	9.346	23.58±2.38	1.77±0.02	4.96±0.02	4.19±0.03	0.60±0.24	0.73±0.19	0.57±0.15	2x400	82	18072014	0
	W2033	18:18:28.1	-18:24:35.0	13.76	15.52	11.96	9.449	28.50±2.89	1.66±0.03	4.90±0.02	3.59±0.03	0.36±0.23	0.46±0.18	0.27±0.14	2x400	79	18072014	0
	W2215	18:18:26.3	-18:24:00.0	13.40	15.17	11.63	9.039	27.48±2.40	1.57±0.02	4.94±0.02	4.18±0.03	0.44±0.24	0.59±0.18	0.34±0.15	2x400	88	18072014	0
	W2249	18:18:26.2	-18:25:37.6	13.20	14.67	11.53	9.228	33.04±4.14	1.80±0.02	4.77±0.03	3.68±0.05	0.20±0.24	0.38±0.18	0.26±0.14	2x350s	88	19072014	0
	W2252	18:18:25.9	-18:23:54.0	13.63	15.43	11.78	9.155	25.83±1.68	1.51±0.03	5.22±0.02	3.58±0.05	0.37±0.24	0.47±0.18	0.26±0.15	2x400	75	18072014	0
	W2352	18:18:25.2	-18:25:01.0	13.65	15.17	11.89	9.403	24.44±2.42	1.60±0.03	4.51±0.02	4.60±0.03	0.54±0.24	0.67±0.18	0.50±0.15	2x400	68	19072014	0
	W2438	18:18:24.5	-18:25:44.4	13.17	15.4	10.75	7.469	19.32±3.10	1.87±0.02	5.24±0.01	3.78±0.02	0.43±0.24	0.40±0.19	0.07±0.15	2x400	118	19072014	0
	W2492	18:18:23.9	-18:26:19.0	13.49	15.15	11.73	9.079	-50.21±3.74							2x400	69	19072014	1
NGC7245	W0045	22:15:07.8	+54:18:26.9	14.165	15.521	12.712	10.873	-39.48±2.65							2x200	27	19072014	1
	W0055	22:15:17.5	+54:18:12.6	13.109	14.385	11.738	9.952	-69.42±2.78	1.67±0.04	4.66±0.04	3.01±0.04	0.06±0.11	0.13±0.10	0.20±0.10	2x150	40	19072014	0
	W0178	22:15:05.4	+54:22:43.6	13.758	15.006	12.392	9.711	-66.92±3.97	1.67±0.03	3.93±0.04	2.46±0.04	-0.24±0.10	-0.23±0.10	-0.42±0.10	2x120	28	18072014	0
	W0179	22:15:05.4	+54:22:49.4	12.969	14.329	11.574	9.711	-60.81±4.33	1.58±0.06	4.30±0.07	3.02±0.06	-0.16±0.11	-0.10±0.11	-0.05±0.11	2x120	37	18072014	0
	W0205	22:15:14.9	+54:20:04.1	13.866	15.203	12.418	10.550	-64.73±2.38	1.50±0.06	3.69±0.07	2.67±0.07	-0.29±0.10	-0.31±0.10	-0.32±0.10	2x220	38	18072014	0
	W3154	22:14:56.3	+54:21:51.6	13.459	14.831	12.037	10.136	-27.63±1.73							2x200	45	19072014	1
	W3214	22:14:58.9	+54:23:05.4	13.618	14.865	12.276	10.537	-51.73±2.31							2x220	38	18072014	1
	W3391	22:15:09.5	+54:23:52.4	14.295	15.639	12.852	10.932	-12.13±4.55							2x200+2x150	33	18072014	1
	W0073	22:15:04.4	+54:20:18.7	13.265	14.478	11.979	10.328	-18.05±1.66							2x220	54	18072014	1
	W0095	22:15:12.0	+54:21:11.4	13.373	14.666	12.002	10.211	-64.68±3.06	1.98±0.06	4.27±0.05	2.17±0.08	-0.21±0.10	-0.18±0.10	-0.15±0.10	2x220	36	18072014	0

Notes. (0) Cluster member from radial velocity (RGB or RC); (1) cluster non-member from radial velocity; (2) Cluster member from radial velocity (main sequence); (3) Unclear membership.

[a] Identifications taken from WEBDA database, except for NGC 559, which came from Joshi et al. (2014).